New Journal of Physics
The open-access journal for physics

Investigation of the role of plasma channels as waveguides for laser-wakefield accelerators

T P A Ibbotson[1], N Bourgeois[1], T P Rowlands-Rees[1], L S Caballero[1], S I Bajlekov[1], P A Walker[1], S Kneip[2], S P D Mangles[2], S R Nagel[2], C A J Palmer[2], N Delerue[3], G Doucas[3], D Urner[3], O Chekhlov[4], R J Clarke[4], E Divall[4], K Ertel[4], P Foster[4], S J Hawkes[4], C J Hooker[4], B Parry[4], P P Rajeev[4], M J V Streeter[4] and S M Hooker[1,5]

[1] Clarendon Laboratory, Parks Road, Oxford OX1 3PU, UK
[2] The Blackett Laboratory, Imperial College London SW7 2BZ, UK
[3] John Adams Institute for accelerator science, University of Oxford, Oxford, UK
[4] Central Laser Facility, Rutherford Appleton Laboratory, Oxon OX11 0QX, UK
E-mail: simon.hooker@physics.ox.ac.uk

New Journal of Physics **12** (2010) 045008 (14pp)
Received 16 October 2009
Published 30 April 2010
Online at http://www.njp.org/
doi:10.1088/1367-2630/12/4/045008

Abstract. The role of plasma channels as waveguides for laser-wakefield accelerators is discussed in terms of the results of experiments performed with the Astra-Gemini laser, numerical simulations using the code WAKE, and the theory of self-focusing and self-guiding of intense laser beams. It is found that at a given electron density, electron beams can be accelerated using lower laser powers in a waveguide structure than in a gas-jet or cell. The transition between relativistically self-guided and channel-assisted guiding is seen in the simulations and in the behaviour of the production of electron beams. We also show that by improving the quality of the driving laser beam the threshold laser energy required to produce electron beams can be reduced by a factor of almost 2. The use of an aperture allows the production of a quasi-monoenergetic electron beam of energy 520 MeV with an input laser power of only 30 TW.

[5] Author to whom any correspondence should be addressed.

Contents

1. Introduction

As first proposed by Tajima and Dawson in 1979 [1], the relativistic plasma wave driven by the interaction of an intense laser pulse with a plasma can be used to accelerate charged particles. These longitudinal electric fields within the wake can be as high as 100 GV m^{-1}, a factor of 1000 higher than in conventional accelerators, making plasma accelerators a very compact source of high-energy particle beams.

The first quasi-monoenergetic beams of electrons from plasma accelerators were reported in 2004 by several groups, employing either plasma channels [2] or gas-jets [3,4]. Since then the energy of the beams has been increased up to the GeV level, by channelling the driving laser pulse with a plasma channel [5,6] or by relativistic self-guiding [7].

In this paper, we discuss the role of plasma channels as waveguides for laser-wakefield accelerators in terms of the results of experiments performed with the Astra-Gemini laser at the Rutherford Appleton Laboratory, numerical simulations, and the theory of self-focusing and self-guiding of intense laser beams. We show that at a given electron density, electron beams can be generated in a waveguide structure at lower laser powers than in a gas-jet or cell. The transition between relativistically self-guided and channel-assisted guiding is seen in the simulations and in the experimentally observed behaviour of the production of electron beams. We demonstrate the importance of the quality of the driving laser beam by showing that the threshold laser energy required to produce electron beams can be reduced by a factor of almost 2 by improving the quality of the focal spot.

The paper is arranged as follows. In section 2, the theory of relativistic self-guiding is reviewed, and in section 3, the experimental arrangement employed is described. In sections 4 and 5, we describe the results of these experiments, and we present in detail the properties of the electron beams generated and the behaviour of the laser radiation transmitted through the plasma channel. The effect of improving the quality of the focal spot of the driving laser is described and explained by numerical simulations in section 6.

2. Self-focusing and self-guiding

The quiver motion of the electrons in the electric field of a laser pulse becomes relativistic when the normalized vector potential $a_0 = eA/m_e c$ is greater than 1. The refractive index of a plasma

is given by $\eta = (1 - (\omega_p^2/\gamma\omega_0^2))^{1/2}$, where ω_p is the plasma frequency and ω_0 is the driving laser frequency. For a laser beam which is peaked on its axis, variations in the relativistic factor γ cause the refractive index to be peaked on axis—which has the effect of focusing the laser pulse. The critical laser power P_c for this focusing to balance diffraction is usually taken to be $P_0 > P_c = 17.4(\omega_0/\omega_p)^2$ GW [8]. This condition is necessary but not sufficient for the laser pulse to be self-guided since transverse density gradients formed at the front of the pulse by the ponderomotive force almost perfectly cancel out self-focusing, so that in the absence of external guiding the front of the pulse diffracts essentially freely.

Lu *et al* [9] have shown that a laser pulse will self-focus to a spot size $w_{sf} \equiv 2k_p^{-1}\sqrt{a_0}$, where $k_p = \omega_p/c$. A laser pulse of power P focused to a spot size w_{sf} has a value of a_0 given by [9]

$$a_0 = 2\,(P/P_c)^{1/3}\,. \tag{1}$$

If the rate of erosion of the leading edge of the pulse by diffraction is slower than that caused by transfer of laser energy to the plasma wave, the pulse can be said to be self-guided. This leads to a condition on a_0 for self-guiding of $a_0 > (\omega_0/\omega_p)^{2/5}$, which can be combined with equation (1) to give a condition on the peak power for self-guiding of

$$P_0 \gtrsim P_c^{\rm diff} = (1/8)(\omega_0/\omega_p)^{6/5} P_c. \tag{2}$$

For the pulse to propagate through the plasma $\omega_0 > \omega_p$, and hence $P_c^{\rm diff} > P_c$. A waveguide with a matched spot size $w_m = w_{sf}$ relaxes this condition to $P_0 \gtrsim P_c$ since diffraction of the leading edge is eliminated. In the case of a waveguide with a matched spot size $w_m > w_{sf}$ diffraction of the leading edge is still reduced, and as we show below, laser pulses with $P_0 < P_c^{\rm diff}$ can still be guided with a spot size close to w_{sf}.

Figure 1 shows the results of simulations performed using the three-dimensional (3D) axi-symmetric particle-in-cell (PIC) code WAKE [10]. Here the propagation of the laser pulse is compared in two cases: (i) a uniform, fully ionized plasma and (ii) a fully ionized plasma channel with a lowest-order mode of 41 μm full-width at half-maximum (FWHM). In both cases $P_0 = 22$ TW, $P_c = 17$ TW and $P_c^{\rm diff} = 131$ TW. The simulations show that without an external guiding structure the laser pulse initially self-focuses to a spot size of approximately w_{sf}, but then diffracts freely as predicted. However, in a plasma channel, the pulse spot size evolves to approximately w_{sf} and maintains this value over many Rayleigh ranges. For the plasma channel a_0 increases beyond that achieved when the pulse is first self-focused owing to compression of the pulse duration. For the simulations of figure 1, this allows a_0 to evolve sufficiently to reach the threshold for injection of electrons into the wake, which is estimated to occur at $a_0 \approx 3$–4 [9, 11, 12]. For a given electron density, and hence output electron beam energy, this allows injection to occur at lower laser powers than without a guiding mechanism in addition to self-focusing.

3. Experimental set-up

In the work described in this paper, the plasma-channel was created using the hydrogen-filled capillary discharge waveguide [13, 14]. For this experiment, the capillary was 33 mm long and 200 μm in diameter. It was connected via gas-slots of diameter 650 μm, located 4 mm from either end of the capillary, to a reservoir filled with hydrogen gas. The gas was allowed to flow for 2.5 s so that a steady state within the capillary was reached before a 1.7 nF capacitor,

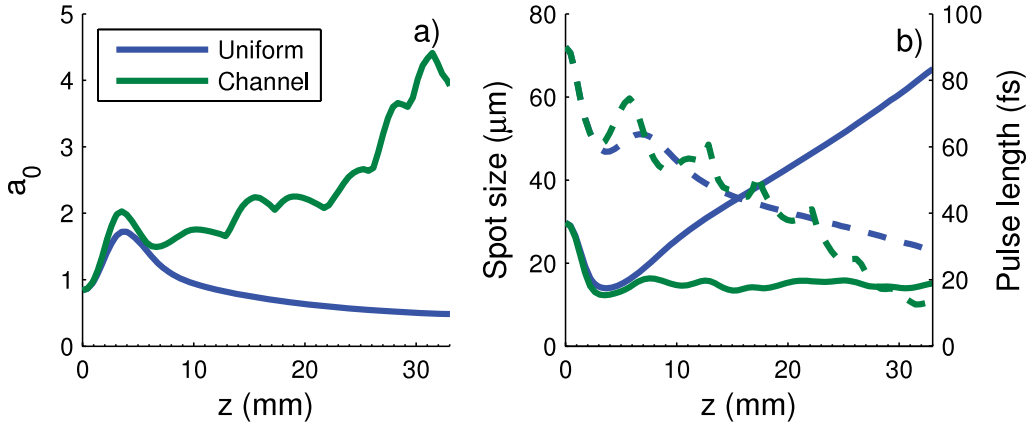

Figure 1. Calculated values, as a function of propagation distance z, of: (a) the peak a_0, (b) the mean spot size (solid) and FWHM duration (dashed) of laser pulses propagating through a gas-cell (blue) and a plasma channel (green). For these calculations, the plasma channel was taken to be parabolic, with an axial electron density of $n_e = 1.8 \times 10^{18}\,\mathrm{cm}^{-3}$ and lowest-order mode of 41 μm FWHM; the gas in the cell was fully ionized, with a uniform electron density of $n_e(0)$; the temporal and transverse spatial profiles of the input laser pulses were Gaussian, with initial FWHM duration of 90 fs and focal spots of 35 μm. The input laser energy in both cases was 2 J corresponding to a peak power of 22 TW.

Table 1. Axial electron densities n_e and matched spot sizes w_m calculated from the scaling laws in [17] for the pressures P presented in this paper.

P (mbar)	n_e ($\times 10^{18}\,\mathrm{cm}^{-3}$)	w_m FWHM (μm)
50	1.2	42
80	1.8	38
95	2.2	37
110	2.5	36
200	4.4	32

charged to 25 kV, was connected across copper electrodes located at either end of the capillary. The resulting current pulse had a peak amplitude of approximately 500 A and a duration ~ 200 ns. The mechanisms by which the capillary discharge establishes a plasma channel have been described previously [15, 16]. Briefly, heat conduction within the plasma establishes a transverse temperature profile with a maximum on axis. Consequently the electron density profile exhibits a minimum on axis there by forming a plasma channel. The transverse profile of the electron density within the plasma channel has been measured interferometrically [17], and from these measurements scaling laws have been deduced for the axial electron density n_e and the matched spot size w_m of the channel. These parameters are given in table 1 for the range of hydrogen backing pressures P employed in the present experiments. It should be noted that the

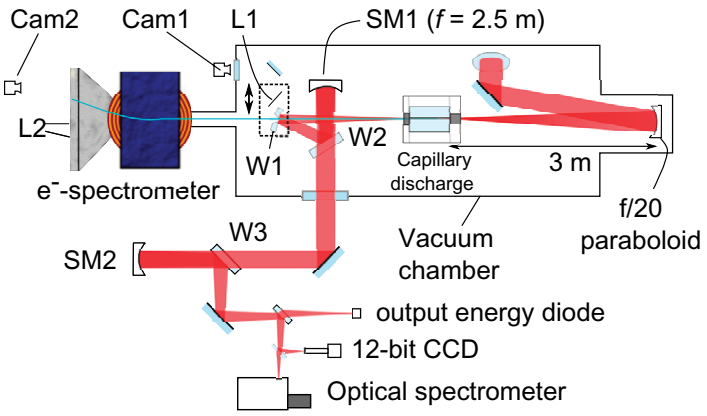

Figure 2. Schematic diagram of the experimental layout.

scaling laws refer to the optimum channel formed during the discharge pulse; at other times the axial density is likely to be lower and the matched spot larger than the quoted values.

The experimental arrangement employed is shown in figure 2. For this experiment, the Astra-Gemini laser delivered pulses of duration 80 ± 5 fs. A paraboloid, with a focal length of 3 m and used at f/20, focused the pulses to a spot size of 22 μm (FWHM) at the entrance to the capillary. A soft aperture could be placed in the beam to better match to the plasma channel and to improve the focal spot quality. Figure 3 shows the transverse profile of the laser focus measured with and without the aperture in place. The aperture increased the spot size of the focus to 35 μm (FWHM) and removed structure in the wings of the focus. However, the use of the aperture restricted the maximum on-target energy to 3 J. Data were taken both with and without the aperture in place.

A wedge (W1), in which a 5 mm diameter hole had been drilled, was placed approximately 1.6 m from the exit of the capillary. Electrons passing through the hole in W1 were dispersed by an electromagnet with an effective field radius R_{eff} of 167 mm and magnet field strength 0.67 T, and detected by a lanex screen (L2) and 12-bit camera (Cam2). Wedge W1 could be replaced by a lanex screen (L1) to measure the transverse profile of the electron beams.

Laser light reflected from the front surface of W1 was reflected by another wedge (W2) onto a spherical mirror (SM1), of focal length 2.5 m, arranged as a retro-reflector to collimate the beam. The collimated beam passed through W2 and out of the vacuum chamber via another wedge reflection (not shown). The transmitted beam passed through another wedge (W3) onto a spherical mirror (SM2), identical to SM1, and directed to several diagnostics via wedge W3. After further reflections from a wedge and a dielectric beam-splitter, the exit plane of the capillary was imaged by a 5 $\times$ microscope objective onto a 12-bit CCD camera. A portion of the laser beam transmitted through a wedge was focused onto a photodiode, so that the laser energy transmission could be determined by comparing with the signal from a diode earlier in the system. Finally, the beam was focused at the entrance of an optical spectrometer after transmission through the beam-splitter. The range of wavelengths which could be detected by the spectrometer was 527–1100 nm; the spectral response of the spectrometer and associated CCD camera was corrected for by using a calibrated white light source.

The discharge current pulse was measured by a Rogowski coil located close to the storage capacitor. The discharge current was transferred from the storage capacitor to the capillary by a 6 m long, 50 Ω coaxial cable. Since the transit time of this cable is not short compared to

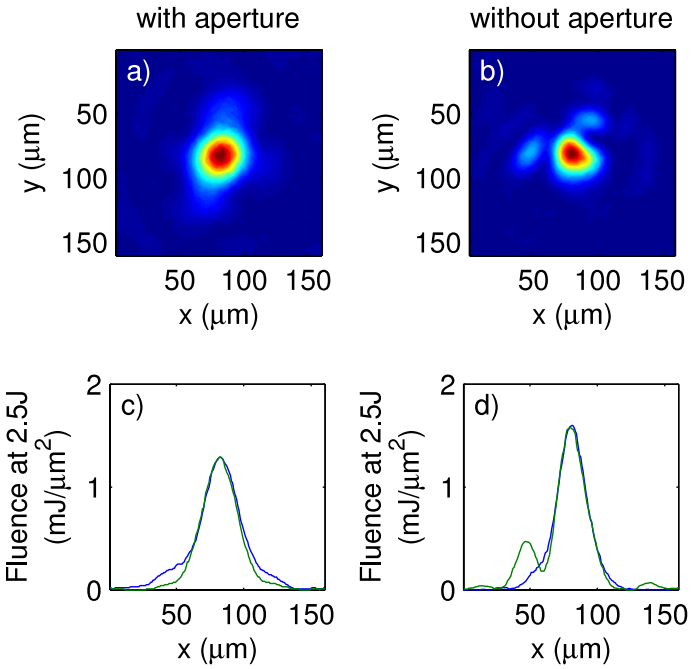

Figure 3. Fluence profiles of the input laser pulse at focus: (a) with the aperture in place and (b) without the aperture. Vertical (blue) and horizontal (green) lineouts are also shown (c, d).

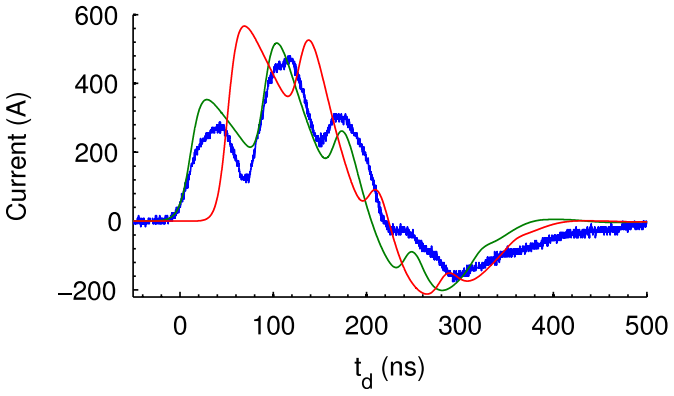

Figure 4. A simulation of the discharge circuit used in this experiment, using the GNUCAP simulation software [18]. The capillary and thyratron switch are modelled by resistors with a time-dependent resistance. The thyratron resistance decays exponentially to represent the switching of the thyratron, and a short time later the capillary resistance also decays exponentially representing the breakdown of the H_2 gas. The current as measured experimentally (blue curve) is plotted along with the simulated current at the same point in the circuit (green curve) and the simulated current flowing through the capillary (red curve).

the duration of the discharge pulse, and the impedance of the cable is not well matched to that of the capillary discharge, strong ringing is evident in the measured current. Further, the measured current will not be the same as that flowing through the capillary. Figure 4 compares

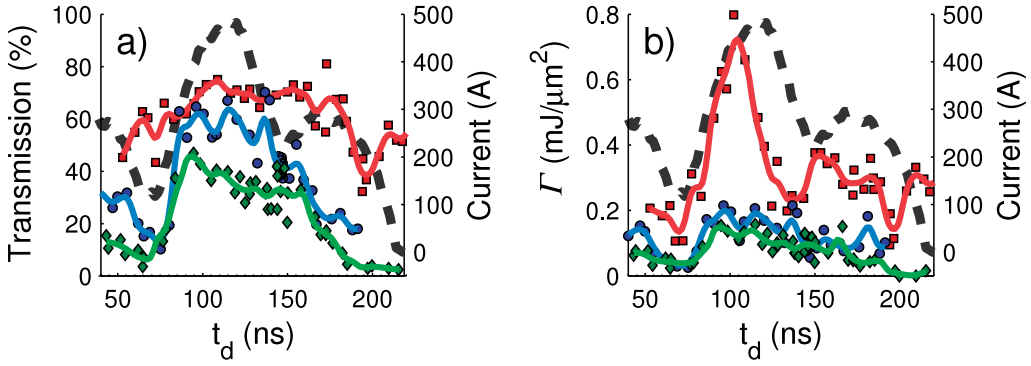

Figure 5. (a) Measured energy transmission and (b) peak fluence Γ of the transmitted laser pulses as a function of delay t_d for $P = 80$ (red), 110 (blue), 200 (green) mbar. The solid lines are a moving average calculated with a Gaussian function, of the form, $e^{-t_d^2/\tau^2}$, where $\tau = 5$ ns. The measured current is given by the dashed line.

simulations of the current flowing through the capacitor and through the capillary, with the measured current flowing through the capacitor. It can be seen that although the peak value and duration of the measured current are similar to that flowing through the capillary, the location of the maxima and minima are different. It is also clear that the current measured for $t_d \lesssim 50$ ns is due to charging of the cables, and does not correspond to current flow through the capillary.

4. Guiding of intense laser pulses

We first present results obtained with the aperture in position and with laser pulses with a mean on-target pulse energy of 2.53 ± 0.15 J and FWHM duration of 80 ± 5 fs, corresponding to a peak normalized vector potential $a_0 \approx 0.9$ at the entrance of the capillary.

Figure 5(a) shows, as a function of delay and for various initial pressures, the measured energy transmission of the laser pulses leaving the waveguide. The transmission is seen to increase with the onset of the discharge current and to remain approximately constant for a period of ~ 100 ns. The peak in the transmission decreases as the pressure increases. A more sensitive measure of the optical guiding is the peak fluence of the transmitted laser radiation, as shown in figure 5(b). This shows that the best guiding was obtained for $P = 80$ mbar: for $t_d \sim 100$ ns, $T \approx 75\%$ and the peak fluence reached $0.80\,\mathrm{mJ}\,\mu\mathrm{m}^{-2}$ compared to a peak input fluence of $1.3\,\mathrm{mJ}\,\mu\mathrm{m}^{-2}$. At longer delays and higher pressures, the peak fluence decreased mostly due to an increase in the measured spot size of the transmitted laser pulse, as can be seen in figure 6.

Figure 5(b) might suggest that at later delays guiding is poor, whereas previous interferometric measurements, and guiding experiments undertaken with lower-power laser pulses, show that a plasma channel is still present at these delays [19]. However, as shown in figure 7, for these delays, the spectra of the transmitted laser pulses were broadened significantly, and consequently chromatic aberration in the microscope objective may have increased the measured spot size of the transmitted pulses, causing an apparent decrease in fluence.

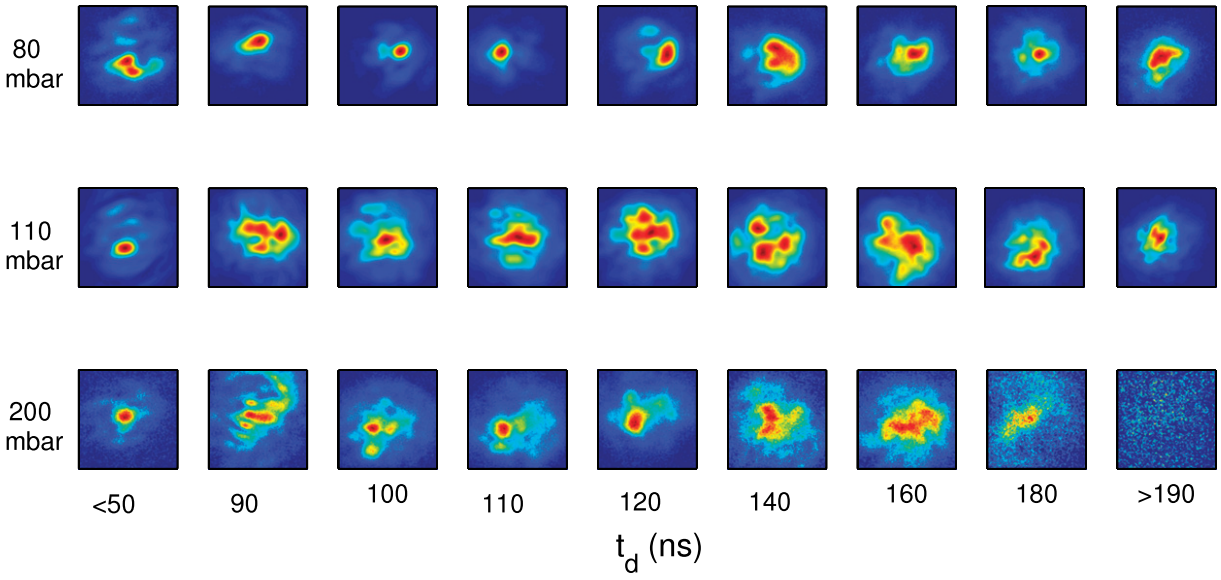

Figure 6. Images of the output fluence profile of the laser pulse at the exit of the capillary as a function of delay and for the same conditions as those shown in figure 5. The colour scale is normalized to the peak of each image. Each image is 200 μm square centred on the capillary exit.

Figure 7 shows the spectra of the transmitted laser pulses as a function of delay t_d. It may be seen that the dominant feature of the spectra is the large amount of red-shifted light, which is consistent with transfer of energy to the plasma wakefield. The amount of red-shifted light increases with t_d and with pressure, suggesting an increased coupling between the laser and the wake at later delays and higher pressures. For all pressures a clear peak is observed at $\sim$20 nm to the blue of the peak of the vacuum spectrum of the laser pulse. We interpret this as an anti-stokes Raman shift, where the expected variation of the shift with electron density is suppressed by relativistic self-focusing [20]. For $t_d > 150$ ns, an appreciable amount of blue-shifted light is also observed. Blue-shifting of the laser pulse can be caused by photon acceleration [21] or by the ionization of partially ionized species [19].

5. Electron beam production

The injection and acceleration of electron beams varied sensitively with t_d, as can be seen in figure 8. For all pressures P, there is little or no charge detected on L1 at delays $t_d < 80$ ns, i.e. when the channel has not yet formed. For $P = 110$ and 200 mbar, electron beams are generated for all $t_d > 80$ ns. However, at lower pressures electron beam production is more sensitive to t_d; for example at $P = 80$ mbar electron beams are only detected for $t_d > 150$ ns. This shows that at lower densities electron beam production depends more critically on the state of the plasma channel.

It should be noted that the charge quoted is the total charge measured on L1, which includes the contribution of low-energy electrons. It is expected that much of the charge measured by L1 is due to the low-energy electrons, which is consistent with the fact that the maximum charge

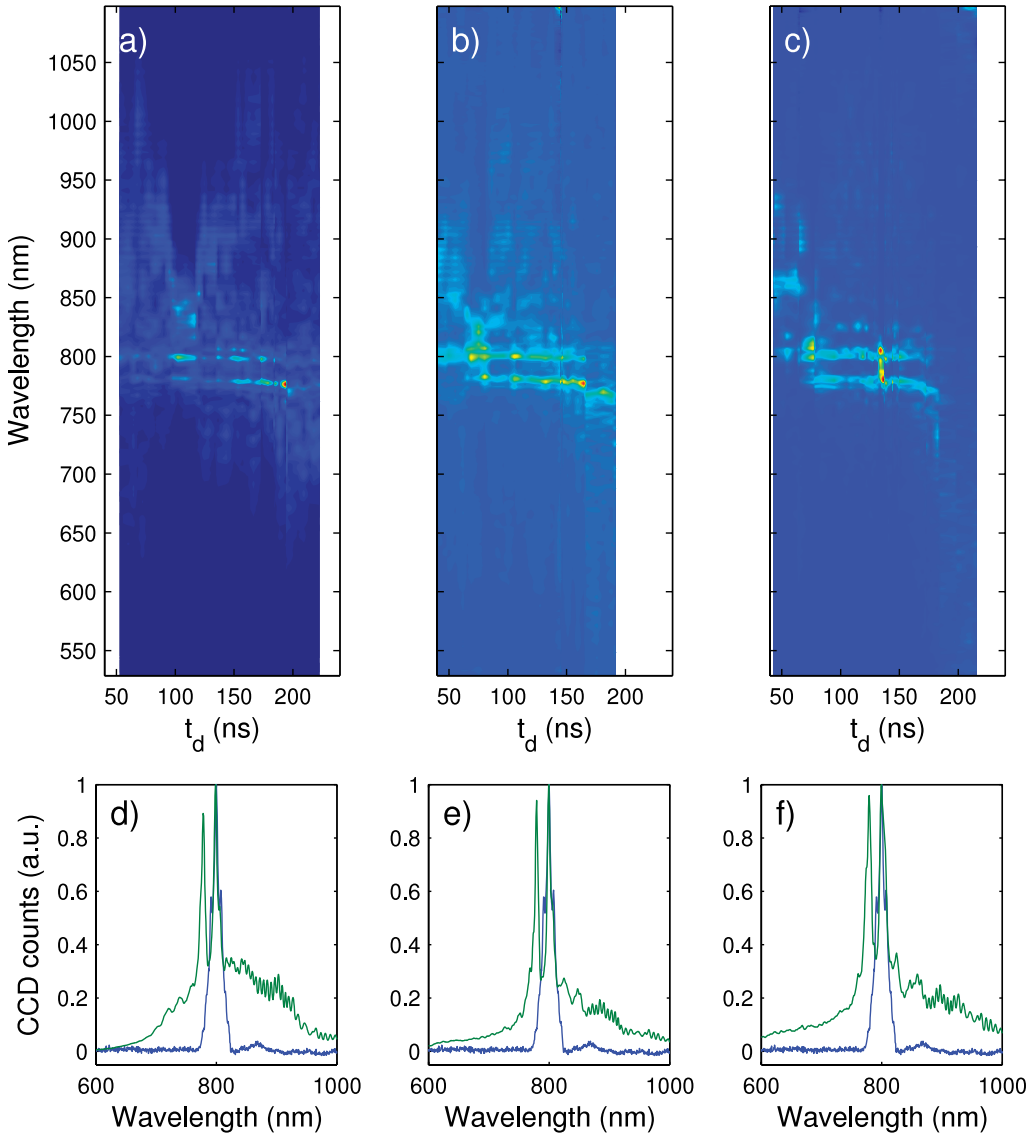

Figure 7. Transmitted laser spectra for $P = 80$, 100 and 200 mbar in (a, d), (b, e) and (c, f), respectively. (a–c) 2D plots of the wavelength of the transmitted light versus delay t_d. For each value of t_d, the spectrum has been normalized to the same value of total energy to remove the effect of varying laser energy transmission so that the trends in the spectra are clearer. (d–f) Lineouts (green) of the spectra shown in (a–c) summed along the t_d-axis, plotted along with the vacuum spectrum (blue).

measured on L2 (which only measures the charge of electrons with energy >100 MeV) was 200 pC.

For the beams at 80 mbar shown in figure 8, the maximum beam energy E_{max} was 540 MeV; the mean beam divergence (1/e full-width) in the horizontal ($\Delta\theta_H$) and vertical ($\Delta\theta_V$) directions was 3.9 ± 0.8 mrad and 5.4 ± 1.3 mrad, respectively, where the errors are the standard deviation; the rms variation in beam pointing was 4.6 and 2.4 mrad in the horizontal (σ_H) and vertical (σ_V)

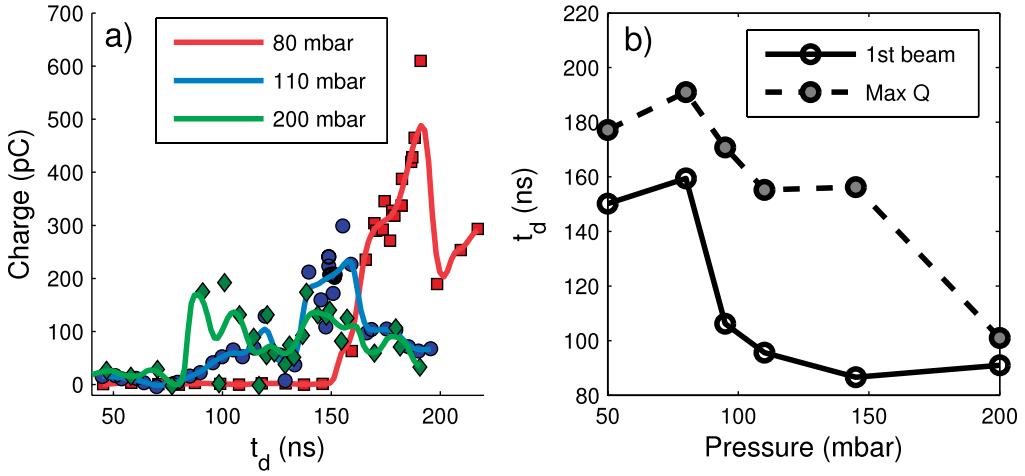

Figure 8. Total electron beam charge Q measured on L1 as a function of delay t_d for $P = 80$, 110 and 200 mbar. The solid lines are a moving Gaussian average as in figure 5. Inset: delay t_d at which electron beams were first observed, and delay at which the highest bunch charge Q was observed, as a function of P.

directions, respectively. By comparison, at 200 mbar, $E_{max} = 410$ MeV; $\Delta\theta_H = 13.9 \pm 3.7$ mrad and $\Delta\theta_V = 16.0 \pm 3.7$ mrad with $\sigma_H = 1$ mrad and $\sigma_V = 1.5$ mrad.

These results may be interpreted in terms of the discussion presented in section 2. For $P = 80$ mbar ($n_e = 1.8 \times 10^{18}$ cm^{-3}), we find $P_0 \approx 1.7 P_c$ and $P_c^{diff} = 7.7 P_c$, and hence the condition for self-guiding is not satisfied. In contrast, for $P = 200$ mbar ($n_e = 4.4 \times 10^{18}$ cm^{-3}), we have $P_0 \approx 4.2 P_c$ and $P_c^{diff} = 4.5 P_c$, which is close to satisfying the self-guiding condition. Thus, it would be expected that for $P \gtrsim 200$ mbar relativistic self-focusing would play a bigger role in the laser propagation than the plasma channel, and hence the propagation of the laser pulse would be similar to that in a gas-jet or cell at the same density. However, at lower densities the plasma channel should play a more significant role in the propagation of the driving laser pulses, and in the development of the wakefield. Given that, for the laser pulses used in this work, self-guiding is required to reach the conditions for electron injection, as discussed below, this explains the observation that for $P \approx 200$ mbar electron beams were generated over a wide range of delays t_d—behaviour more characteristic of a gas-cell—whereas at lower pressures injection was much more sensitive to the delay t_d, consistent with an evolving plasma channel. The sensitivity to t_d may be caused by evolution of the longitudinal and transverse density profiles of the plasma channel during the discharge pulse; it has also been shown that ionization might assist electron injection at delays t_d for which the plasma is partially ionized [19], and the degree of ionization will vary with t_d.

Figure 9 shows measured electron energy spectra for various P at delays t_d corresponding to optimum beam generation. The beam energy is maximized and the energy spread minimized at $P = 80$ mbar, where the beam energy was measured to be 520 MeV with a beam charge of 70 pC. The effect of the electron beam divergence on the measured energy spectrum was assessed by employing a modified Richardson–Lucy algorithm. Taking the angular divergence of the beam in the energy-dispersed direction to equal that measured in the non-dispersed direction, this procedure suggests that the relative energy spread of the beam in less than 5%.

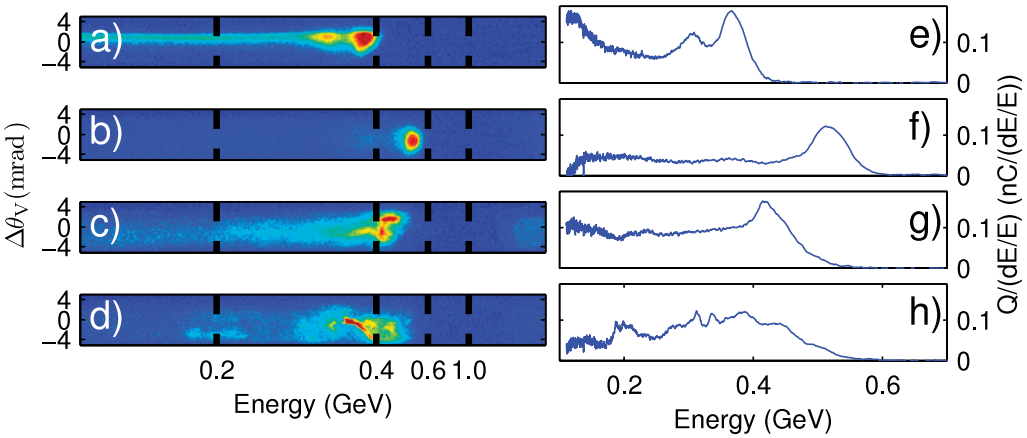

Figure 9. Raw electron energy spectra (a–d) showing the fluorescence from L2, and spectra in units of charge per relative energy spread (e–h) for: (a, e) $P = 50$ mbar, $t_d = 147$ ns; (b, f) $P = 80$ mbar, $t_d = 189$ ns; (c, g) $P = 110$ mbar, $t_d = 181$ ns; (d, h) $P = 200$ mbar, $t_d = 150$ ns.

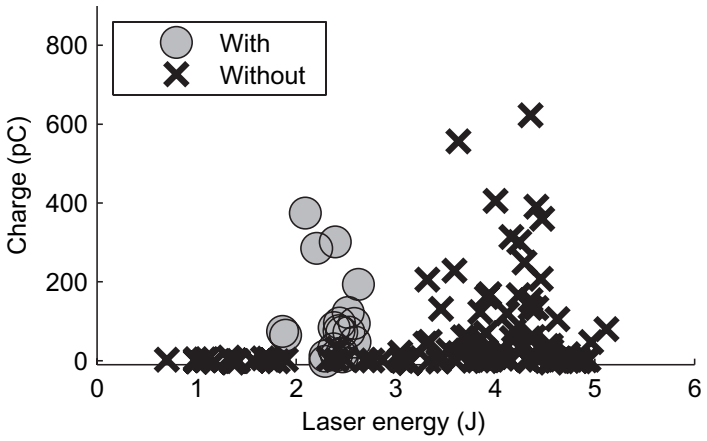

Figure 10. Total electron beam charge Q measured on L1 as a function of input laser energy and various delays t_d with and without the aperture in position, for $P = 95$ mbar.

This may be taken as an upper limit since the deconvolution routine uses a braking function designed to give the most pessimistic solution consistent with the data [22].

We note that the long, narrow divergence tail seen in the energy spectrum recorded for $P = 50$ mbar could be a signature of ionization-induced injection. This was previously suggested as a possible explanation for the observed sensitivity to t_d of electron beam production in a capillary waveguide operated at low pressures [19]; further investigation is required to determine if this is the case.

6. Effect of the transverse profile of the input laser spot

Figure 10 shows the electron beam charge measured on L1 for data taken both with and without the aperture in place. It can clearly be seen that without the aperture electron beams were

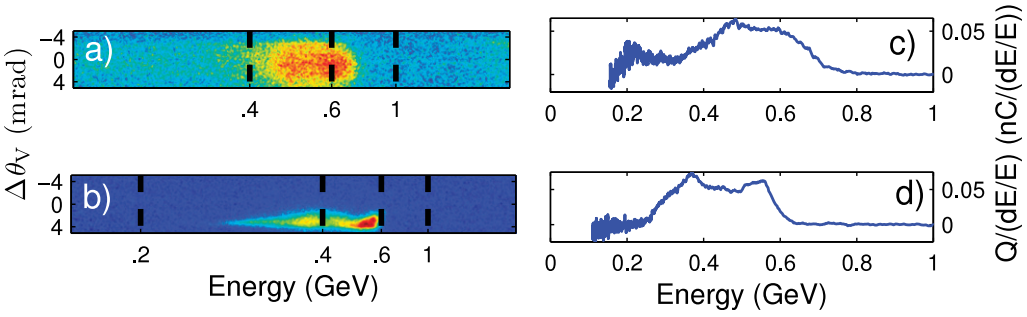

Figure 11. Electron energy spectra (a, c) without the aperture in place and an input laser energy of 3.5 J and (b, d) with the aperture and an input laser energy of 2.5 J. The electron beam in (a) has been significantly scattered by passing through lanex screen L1 which was on axis for that shot.

only produced for laser energies $\gtrsim$3.5 J, but with the aperture electron beams were produced with input laser energies as low as 2 J. Figure 11 shows electron energy spectra recorded for $P = 95$ mbar with and without the aperture in place. Both beams have an energy >500 MeV, even though with the aperture in place the energy on target was lower by a factor of 1.4. The observed reduction of laser energy required to generate electron beams when the aperture is employed could in principle be due to better matching of the input laser spot to the matched spot of the plasma channel, or to improvement of the transverse spatial profile of the input beam.

Figure 12 shows simulations using the code WAKE, which further help to explain the behaviour of electron beam production. Figures 12(a) and (d) show the effect of different input focal spot sizes with the same input energy of 2.5 J. It can be seen that the evolution of a_0 is similar in both cases and both reach the threshold for self-injection of $a_0 \approx 3$–4 at similar propagation distances. The reduction of laser energy required to generate an electron beam when an aperture is employed cannot therefore be due to better matching of the spot size of the input pulse to the matched spot size of the channel. Figures 12(b) and (e) show the calculated pulse parameters for Gaussian input pulses with a focal spot size equal to that generated without the aperture, and pulse energies adjusted to give the measured axial fluences for total on-target energies of 2.5 and 4.0 J. It can be seen that, in agreement with the results of section 6, for the higher pulse energy a0 just reaches the threshold for electron injection, but that this is not the case for the lower energy pulse. Taken together, the results of figures 12(a), (b), (d) and (e) show that the improved performance observed with the aperture arises from the higher proportion of energy residing in the central part of the laser focus—i.e. an improvement in the quality of the input beam—rather than better matching of the spot size to the channel.

Figures 12(c) and (f) show the effect of changing the axial electron density for input pulses of the same energy and spot size. The point at which the threshold for injection of electrons into the wake is reached occurs at shorter propagation distances with increasing axial electron density. At a density corresponding to 200 mbar it can be seen that the threshold is reached as soon as the pulse has self-focused and no further evolution of the pulse is required to reach it. This would imply that at these conditions the behaviour of electron beam production would be fairly insensitive to the state of the plasma channel, as observed in figure 8.

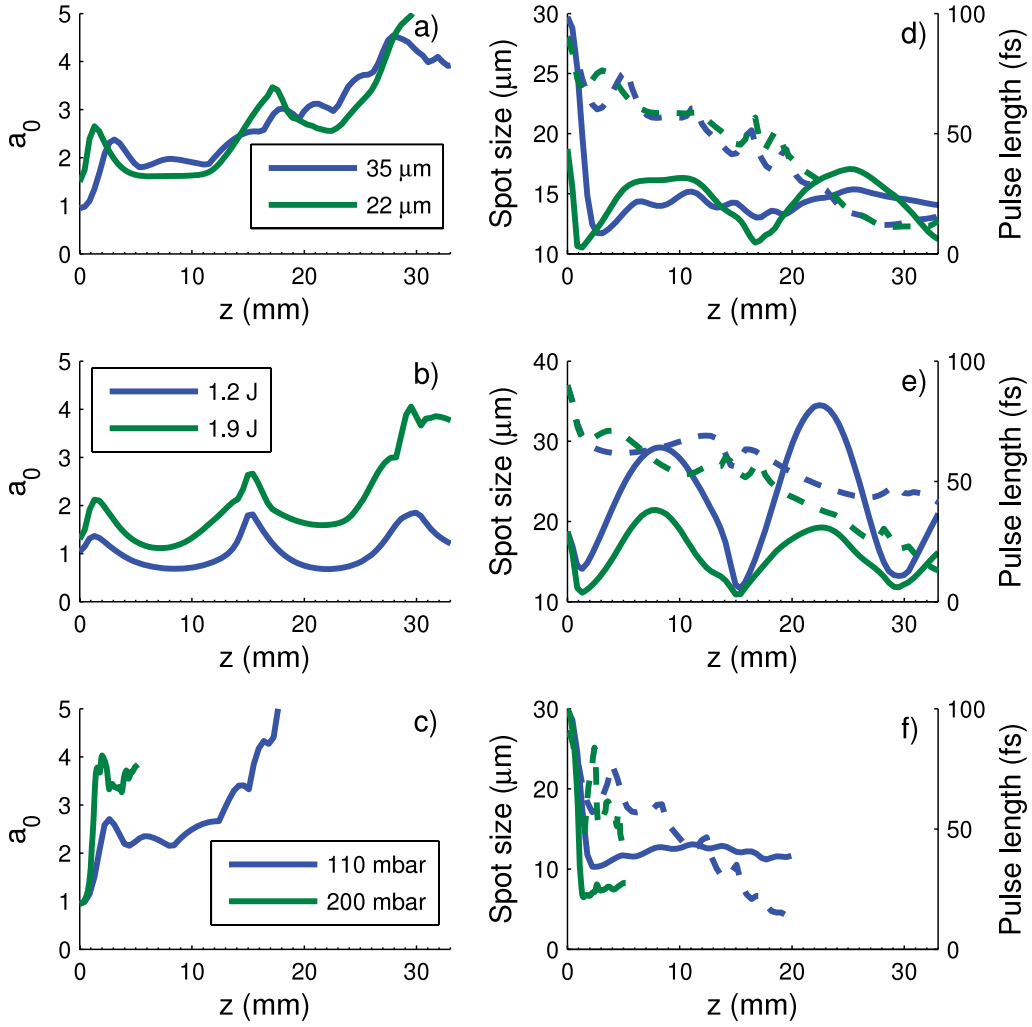

Figure 12. Calculated values, as a function of propagation distance z, of: (a–c) the peak a_0, (d–f) the mean spot size (solid) and FWHM duration (dashed) of laser pulses propagating through a plasma channel. For these calculations, the plasma channel was parabolic and the temporal and spatial profiles of the input laser pulses were Gaussian, the initial FWHM duration of the laser pulse was 90 fs in all cases. (a, d) Input laser focal spot size was 35 μm (blue) and 22 μm (green) with an energy of 2.5 J. (b, e) An input laser focal spot size of 22 μm (no aperture) and pulse energy of 1.2 J (blue) and 1.9 J (green), to give axial fluences matching the measured values for total on-target energies of 2.5 and 4 J, respectively. (c, f) An input laser pulse of energy 2.5 J and spot size of 35 μm and an axial electron density of 2.2×10^{18} cm^{-3} (blue) and 4.4×10^{18} cm^{-3} (green), corresponding to $P = 110$ and 200 mbar, respectively.

7. Conclusions and future work

In conclusion, quasi-monoenergetic electron beams with energies above 0.5 GeV were generated with input laser pulses of only 2.7 J and peak power of 30 TW, using plasma channels with an axial density as low as 1.8×10^{18} cm^{-3}. We demonstrated through simulations that laser

pulses with $P_c < P \lesssim P_c^{diff}$ will, in a plasma channel with $w_m > w_{sf}$, self-focus and propagate stably with a near-constant spot size approximately equal to w_{sf}. In contrast, in a gas-cell or jet laser pulses with $P < P_c^{diff}$ focus to a spot of order w_{sf}, but thereafter diffract, reducing a_0. These differences mean that a plasma channel allows a_0 to increase through temporal compression to the point that self-injection occurs for laser powers and plasma densities too low to achieve electron injection in a gas-jet or cell. The transition between relativistically self-guided and channel-assisted guiding was observed in the behaviour of the production of electron beams. We have also shown experimentally that the generation of electron beams depends strongly on the properties of the input laser spot. Improving the focal spot quality with a soft aperture reduced by a factor of almost 2 the input laser energy required to produce electron beams. Taken together, these results suggest that guiding high-quality driving laser pulses in plasma channels will enable high-energy quasi-monoenergetic electron beams to be generated from relatively small-scale laser systems.

Acknowledgments

We acknowledge the support of the UK Engineering and Physical Sciences Research Council (grant EP/C005449) and the European Community-New and Emerging Science and Technology Activity under the FP6 'Structuring the European Research Area' programme (project EuroLEAP, contract number 028514).

References

[1] Tajima T and Dawson J M 1979 *Phys. Rev. Lett.* **43** 267
[2] Geddes C G R *et al* 2004 *Nature* **431** 538
[3] Mangles S P D *et al* 2004 *Nature* **431** 535
[4] Faure J *et al* 2004 *Nature* **431** 541
[5] Leemans W P *et al* 2006 *Nat. Phys.* **2** 696
[6] Nakamura K *et al* 2007 *Phys. Plasmas* **14** 056708
[7] Kneip S *et al* 2009 *Phys. Rev. Lett.* **103** 035002
[8] Esarey E *et al* 2002 *IEEE J. Quantum Electron.* **33** 1879
[9] Lu W *et al* 2007 *Phys. Rev. Acc. ST Beams* **10** 061301
[10] Mora P and Antonsen Jr T M 1997 *Phys. Plasmas* **4** 217
[11] Mangles S P D *et al* 2007 *Phys. Plasmas* **14** 056702
[12] Mangles S P D *et al* 2008 *IEEE Trans. Plasma Sci.* **36** 1715
[13] Spence D J and Hooker S M 2000 *Phys. Rev.* E **63** 015401
[14] Butler A, Spence D J and Hooker S M 2002 *Phys. Rev. Lett.* **89** 185003
[15] Bobrova N A *et al* 2001 *Phys. Rev.* E **65** 016407
[16] Broks B H P, Garloff K and van der Mullen J J A M 2005 *Phys. Rev.* E **71** 016401
[17] Gonsalves A J *et al* 2007 *Phys. Rev. Lett.* **98** 025002
[18] Davis A *Gnucap: An Analog and Mixed Signal Circuit Simulator* http://wiki.gnucap.org/dokuwiki/doku.php?id=gnucap:start/
[19] Rowlands-Rees T P *et al* 2008 *Phys. Rev. Lett.* **100** 105005
[20] Hooker S M Ibbotson T P A Bourgeois N Experimental observation of relativistically damped Raman shifts in preparation
[21] Mori W B 1997 *IEEE J. Quantum Electron.* **33** 1942
[22] Rowlands-Rees T P 2009 Laser wakefield acceleration in the hydrogen-filled capillary discharge waveguide *PhD Thesis* University of Oxford